Ethiopian Journal of Water Science and Technology (EJWST)

DOI: https://doi.org/10.59122/EJWST836

Vol. 9, 2026, Pages: 93~122 ISSN (Print): 2220-7643

Groundwater Flow and Contaminant Transport Modeling in the Selgi Watershed, Woleka Sub Basin, Ethiopia

Wasihun Deribe[1*], Samuel Dagalo[1], Abunu Atlabachew[1]

[1*] Ph. D. Scholar, Faculty of Water Resources and Irrigation Engineering, Water Technology Institute, Arba Minch University, Arba Minch, Ethiopia
[1] Associate Professor, Faculty of Water Resources and Irrigation Engineering, Water Technology Institute, Arba Minch University, Arba Minch, Ethiopia
[1] Associate Professor, Faculty of Water Resources and Irrigation Engineering, Water Technology Institute, Arba Minch University, Arba Minch, Ethiopia
***Corresponding author**: wasihunderibe2199@gmail.com

ABSTRACT

Owing to urbanization, modern agriculture, population growth, and global warming, groundwater supplies are under significant stress. The quality and potential of groundwater have declined over time. In this context, groundwater models are crucial for tracking these changes. This study employs the MODFLOW and MT3DMS models to simulate nitrate concentration and groundwater levels. Data were collected from twelve hand-dug wells every quarter of the year for nitrate concentrations, while eighteen wells provided monthly measurements of groundwater levels. The default metrics found in the Visual MODFLOW 2015 model were utilized to evaluate model performance. After the flow models were calibrated and validated, the results demonstrated a very good fit, and the transport modeling also performed well. A sensitivity analysis using the PEST model indicated that hydraulic conductivity is a sensitive parameter, varying between 0.01 and 0.15 m/day, while other parameters remained constant. The study employed sorption and reaction-type simulations to calibrate the Transport Model owing to the mobility of nitrate species, with advective transport being the predominant mechanism. The ideal parameters for nitrate calibration included a distribution coefficient (Kd) of 0.000001 1/mg/L, a reaction rate of 0.001 1/day, an effective velocity of 0.14 m/day, and a longitudinal dispersion of 100 meters. Hydraulic heads were observed to be low downstream and high upstream in the watershed. Hydraulic heads were observed to be lowest downstream and highest upstream in the watershed. However, only minor changes were noted in the simulated nitrate concentration within the watershed. This finding may assist decision-makers in understanding groundwater level variability and nitrate contamination, which can guide future fertilizer application rates and the development of new shallow wells.

Keywords: Calibration, MODFLOW, MT3DMS, Kd, PEST, and Validation

Received: 25 January, 2026; Accepted: 01 April, 2026 Published: 11 June, 2026

1. INTRODUCTION

Groundwater serves various vital purposes and is one of the primary sources of fresh water on Earth. However, the quality of groundwater has deteriorated over time because of industrialization, urbanization, and agricultural practices. It has become contaminated particularly by non-point source pollutants originating from agricultural areas. The overuse of nitrogen-nitrate can lead to degradation of groundwater quality although it is essential for agricultural production (Filippis et al., 2021). The magnitude and potential impact of groundwater nitrate contamination can be assessed by intrinsic and specific vulnerability methods. The specific vulnerability model evaluates groundwater flow and the transport of contaminants by considering both the susceptibility of the aquifer material and the potential effects of specific pollutants. In contrast, the intrinsic vulnerability method does not consider the impact of individual contaminants (National Research Council, 1993). The process of nitrate leaching into groundwater involves several biochemical changes. These changes include the leaching of nitrates, crop absorption, nitrification, volatilization, immobilization, and mineralization. Groundwater nitrate pollution is an ongoing issue that requires precise analytical and numerical solutions (Jimrise et al., 2022).

Groundwater Models, being simplified representations of a more complex reality, have proven to be valuable tools for addressing various groundwater issues and aiding in decision-making processes. These models examine different hydrogeological conditions by calculating groundwater flow, and estimating the concentration of chemicals in aquifers and subsurface units using various groundwater flow and transport models (Sundararajan & Sankaran, 2020).

Understanding the movement of pollutants in the subsurface environment can be enhanced by modeling groundwater flow and pollutant transport (Sundararaj et al., 2022). Many computational models for mass transport and groundwater flow have been developed over the years, most of which focus on saturated flow in porous media. However, the processes in unsaturated zones are more complex and not as well understood. When groundwater contamination occurs, seepage velocity and mass transfer play crucial roles in numerical groundwater flow models. Finite Difference and Finite Element are the methods most frequently employed to address groundwater flow and mass transport problems. Finite Differences are simple to apply and frequently require fewer elements to build the equation matrix. Handling boundaries with irregular shapes, the Finite

Element method performs better than the Finite Difference technique. Integrated Finite Differences are capable of handling irregular domains just like Finite Elements. When choosing a technique, the user's preferences are usually considered (Karatzas, 2017).

A complete and easy-to-use program for simulating three-dimensional groundwater flow and pollutant transport is Visual MODFLOW. It integrates several modeling components such as MODFLOW, MODPATH, Zone Budget, MT3DMS/RT3D, and WinPEST into a single product that features an intuitive and comprehensive graphical user interface (Waterloo Hydrogeologic, 2009). For the past 22 years, this model had been effectively utilized in various applications (Valivand & Katibeh, 2020; Hariharan & Shankar, 2017; ; Gebreyohannes et al., 2017; Ayenew et al., 2008). Groundwater modeling is a crucial initial step that involves simulating groundwater levels and other important factors, such as hydraulic conductivity and specific storage, before modeling pollutant transport.

In order to prepare the input data of the model, calibration, verification, and sensitivity analysis should be conducted. According to Sundararajan and Sankaran (2020), model calibration and validation are processes that refine the model by progressively enhancing the accuracy and reliability of field estimates for various hydrogeological parameters. During the validation stage, the performance of the calibrated model is assessed using a new dataset that differs from the data used for calibration (Mrinal & Susmita, 2022). Sensitivity analysis is then carried out to identify the parameters that most significantly affect the outcomes (Kumar et al., 2022).

The study area has two cropping seasons: the rainy season and the irrigation season. During these times, farmers apply nitrogen fertilizers twice a year to boost crop production. However, there are no monitoring wells installed in the area to measure groundwater levels or assess groundwater quality parameters. To evaluate fluctuations in groundwater levels and the extent of nitrate contamination, the researchers collected 12 months of groundwater level measurements from 18 hand-dug wells and quarterly nitrate concentration data from 12 hand-dug wells. This information was utilized for groundwater modeling and contaminant transport modeling in the Seligi Watershed.

2. METHODOLOGY

2.1 Description of the Study Area

The Selgi Watershed is located between 39.37° and 39.51° east longitude and 10.71° and 10.92° north latitude in the northeastern part of the Woleka River sub-basin, within the Upper Blue Nile River region. It is situated approximately 450 km from the capital city, Addis Ababa. The watershed spans for an area of 127.72 km² (see Figure 1).

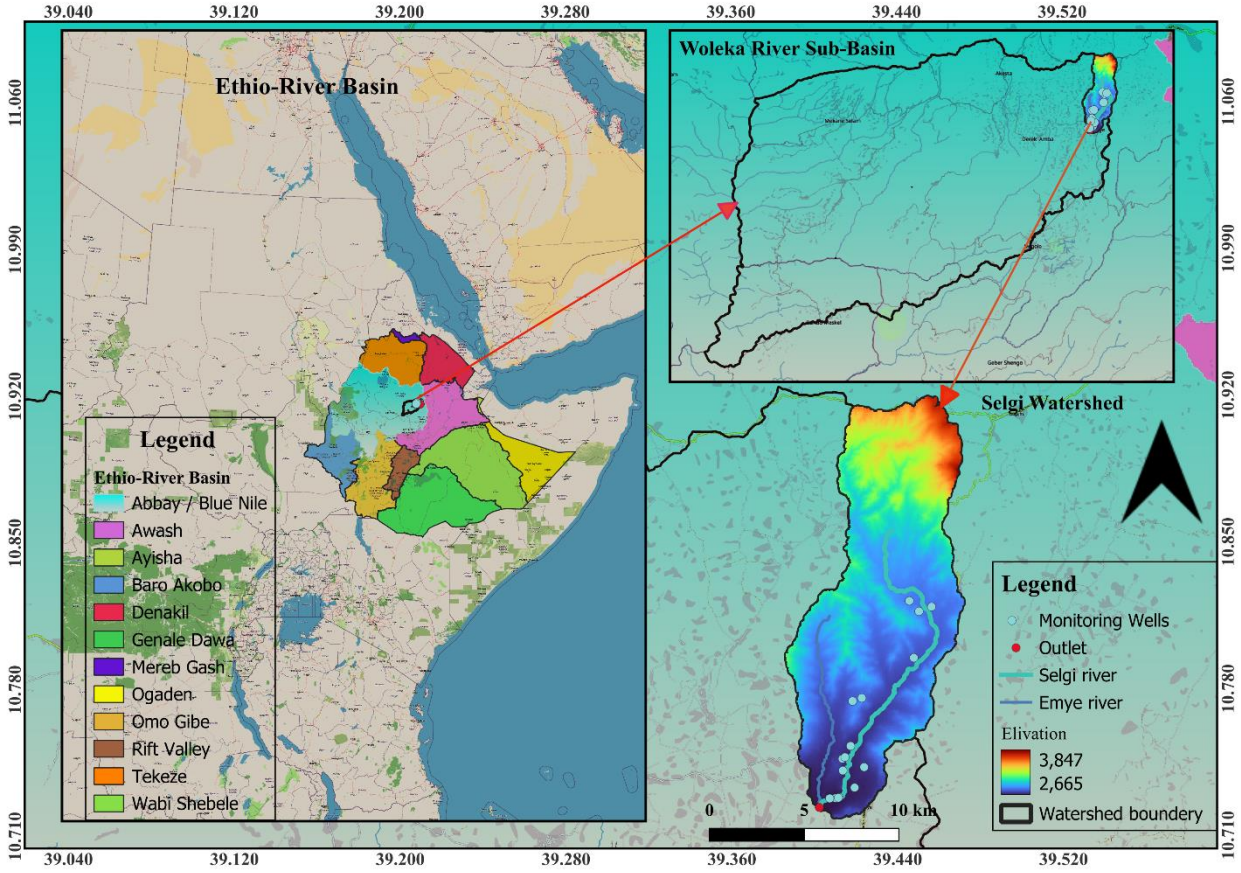

Figure 1. Map of the study area

This watershed has elevations ranging from 2,665 to 3,849 meters above sea level. While the lower regions have gentle riverbank slopes, the upper portion of the watershed is extremely steep. Two streams flow through the watershed from north to south: the Emiye River in the west and the Selgi River, which is the main stream in the east. Selgi River is the main tributary of the Woleka River, also referred to as the Betto River. The watershed experiences a main rainy season during the summer, receiving an average of 1,169 mm of precipitation annually. The area

experiences temperatures from -1 to 29 degrees Celsius. Autumn brings the lowest temperature (Meher), and the start of summer brings the highest temperature (Kiremt).

The geological context of the research area is characterized by basalt formation (see Figure 2). The two most prevalent types of basalt rocks are Tarmaber basalt and Amba Aiba basalt. Tarmaber basalt constitutes the majority of the geological setting in the watershed. According to Tigel et al. (2010), this geological formation can extend up to 500 meters below the surface. The eroded formations of basalt display shades of reddish-brown, light gray, light yellow, and greenish-gray, while the basalt itself has a striking dark gray appearance. It features columnar jointing and a medium to coarse-grained texture. In contrast, the Amba Aiba basalt formation exhibits horizontal failures and a slight degree of weathering, characterized by its columnar and blocky structure. As shown in Figure 2(a), this formation is located in the downstream region of the watershed. These basalt formations can be advantageous for groundwater movement owing to secondary porosity (Tsegaw et al., 2025).

Three different soil textural classes such as clay loam, loam, and heavy clay soil make up the watershed. The majority of the research region is covered by clay loam, which is the predominant soil type. As seen in Figure 2(b), loam soil makes up only a minor portion of the watershed. In the watershed, heavy clay soil is also the most common soil type. While heavy clay soil obstructs water movement within the soil and hampers groundwater recharge, loam and clay loam soils facilitate groundwater movement and recharge efficiently. However, thick clay soil has a higher attenuation potential than the other types of soil when it comes to pollutant transfer (Tsegaw et al., 2026).

The research area land use and land cover map displayed in Figure 2 (c) shows that the predominant soil type is cultivated land. But a sizable portion of land is also deteriorated. The third form of land use along riverbanks is grassland, which is defined as a marshy area by Tsegaw et al. (2026). The upper part of the study area is degraded because of steep slopes, deforestation, and intensive cultivation. In contrast, the lower part of the watershed has fertile soil, with soil depth extending up to 3 meters. This section of the watershed is cultivated twice a year. Irrigation is the second farming practice in the study area, following the main summer season. For this

purpose, more than eight modern small-scale irrigation schemes have been built along the Selgi River. To enhance agricultural production, farmers use nitrogen-based fertilizers.

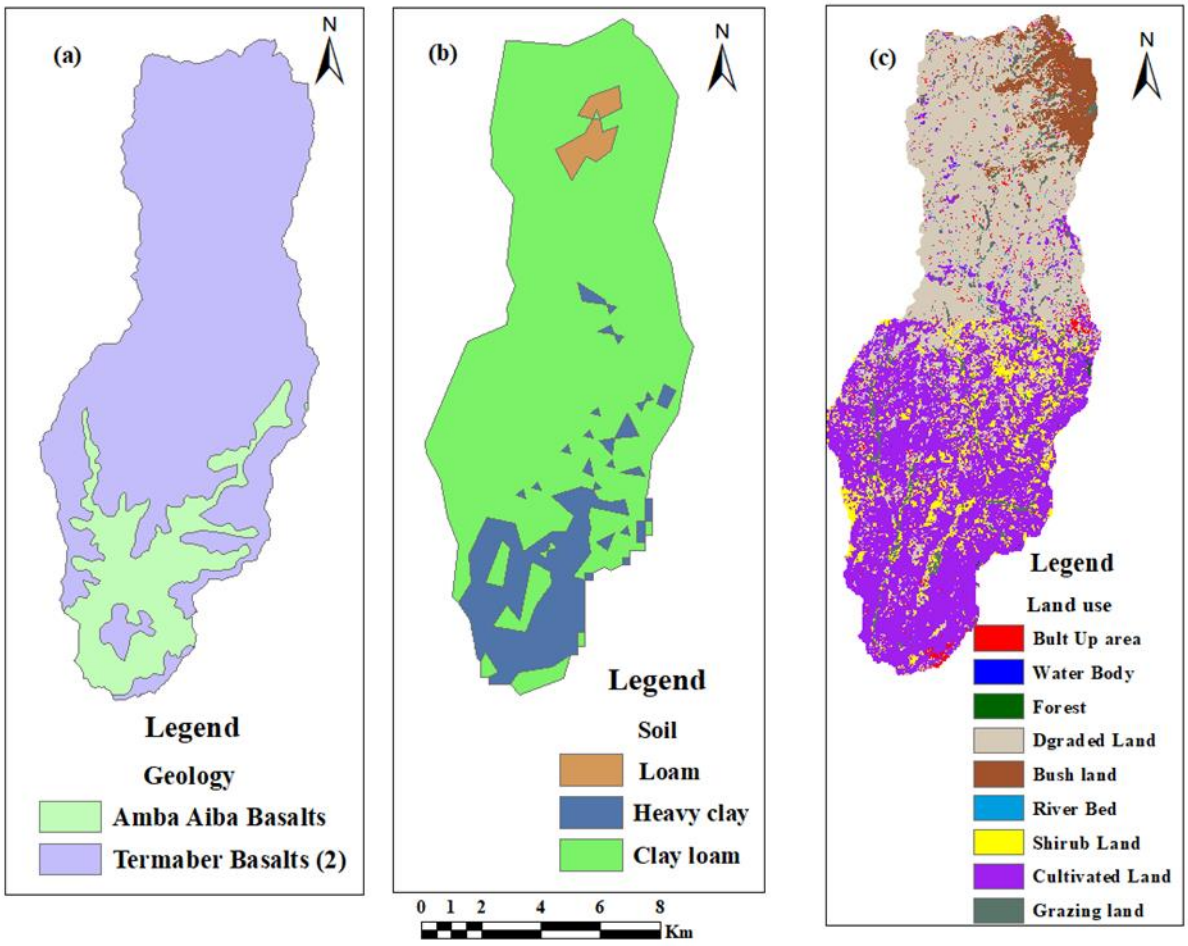

Figure 2. Watershed characteristics map (a) Geology, (b) Soil, and (c) Land use map

In the study area, the main sources of drinking water are a spring and a hand-dug well. Residents living downstream typically use the hand-dug well while those upstream mainly rely on the spring. Additionally, two deep wells have been drilled to provide water for the small city of Kabe, but only one of them is currently operational. Figure 3 illustrates the area's geological structure and outlines the formation of the operational well. The completion report of the well indicated that the upper portion of the aquifer has a high penetration rate, suggesting significant weathering in this area. Key factors related to the aquifer's performance are highlighted in the pumping test report. Key factors related to the aquifer's performance are highlighted in the pumping test report. According to the Theiss analysis method, the groundwater dynamics of the aquifer is evaluated

as: Transmissivity (T) = 3.25 m²/d, hydraulic conductivity (K) = 0.0338 m/d, and storativity (S) = 2.73E-5. However, the Cooper-Jacob analytical approach yields different values: hydraulic conductivity (K) = 0.0269 m/d and transmissivity (T) = 2.58 m²/d.

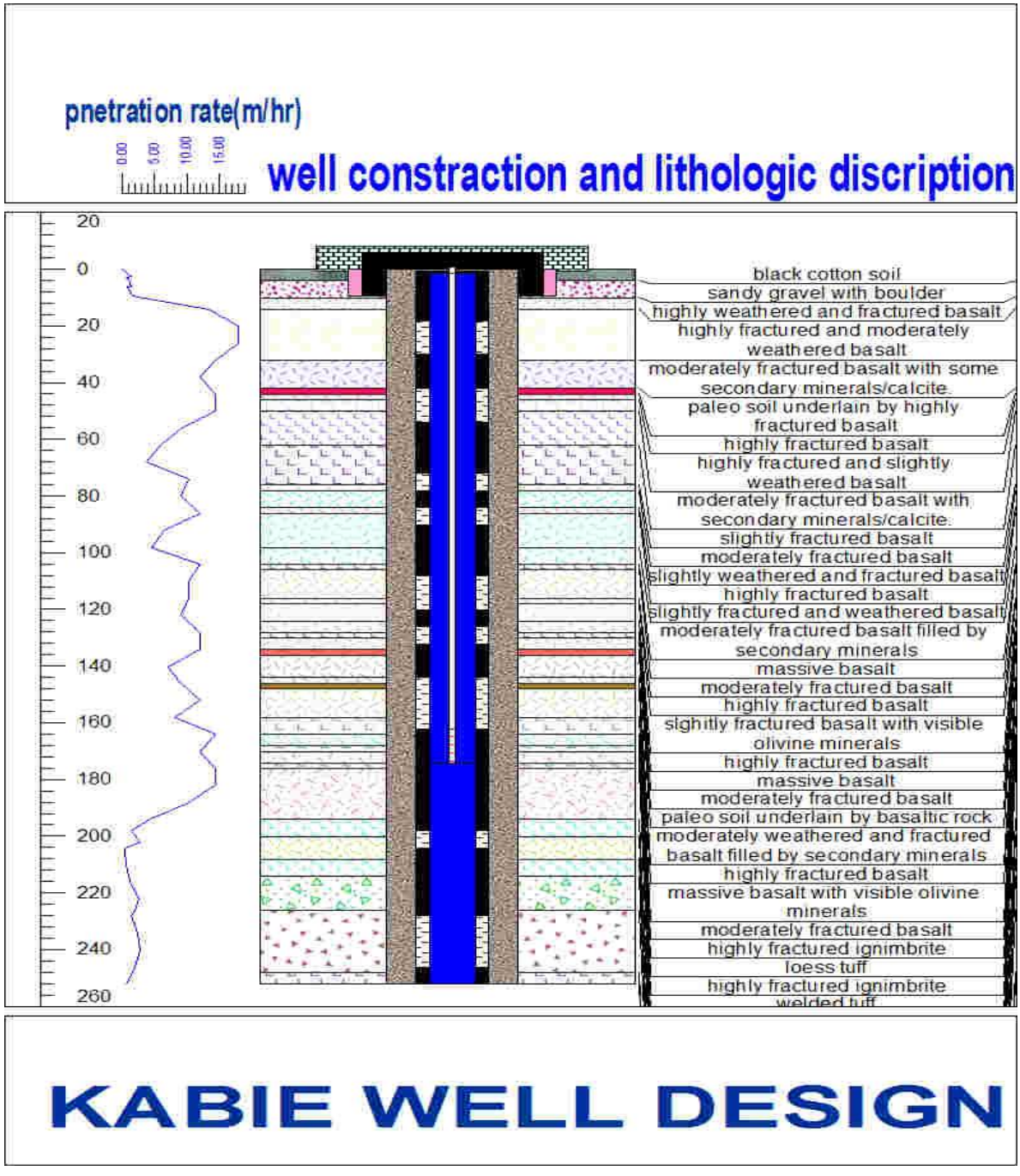

Figure 3. Borehole lithological description at the Kabie well site (Source: Kabie well completion report)

2.2 Data Collection

This study collects both Primary data and secondary data, while the secondary data were utilized to establish the initial parameters. Table 1 provides a detailed overview of the sources and types of data used.

Table 1. Data source and type

No.	Thematic Layers	Data used	Data Sources	Resolution	Software used	Data type
1	Geology	Shapefile	MoWE, 2011	1*1km	GIS	Secondary
2	Soil	Shapefile	http://www.isric.org/data/AfSoilGrids250m	250*250m	GIS	
3	Land Use Land Cover map	Landsat 8 image	USGS Landsat 8 https://earthexplorer.usgs.gov/	30*30m	ERDAS imagine	Secondary
4	Precipitation	Chirps satellite	Satellite (2002-2024)	Monthly	Google engine	Secondary
5	Groundwater head	18 HDW	Observed	Monthly	-	Primary
6	Nitrate concentration	12 Sample	Observed	Quarterly	-	Primary
7	Initial groundwater parameter	Pumping test report	Amhara Design and Supervision Enterprise	-	-	Secondary

The groundwater level was measured using a tape meter early in the morning, before extracting groundwater for domestic purposes. Most hand-dug wells are were not pumped; they are opened to the atmosphere, making it easy to measure the groundwater depth. To collect a water sample for examining nitrate concentration, the groundwater was pumped for more than three minutes to remove any stagnant water from the PVC pipe that holds the pump.

2.3 Visual MODFLOW Flex Model Setup

The GIS-based groundwater vulnerability assessments were limited to predict contaminated flow paths. Groundwater modeling is an effective technique for predicting changes in groundwater levels and contaminant concentrations, especially in situations involving pollution plumes, estimating contamination loads, and assessing aquifer management (Karatzas, 2017). This study evaluates the pollution load of non-point source pollutants using the Visual MODFLOW groundwater model.

2.3.1 Conceptual Model Development

Model setup is an essential step before conducting numerical simulations. In this study, the Visual MODFLOW Flex 2015 program was used to simulate the movement of pollutants and groundwater flow. This program employed two distinct processes for simulating flow and pollutant transport: conceptual modeling and numerical modeling. The conceptual modeling process requires several steps to create a model specific to the study objectives. The initial step is to establish the model's objective and choose the type of model to be simulated. In this study, both flow and transport models have been chosen for the future simulation of flow and contaminant concentration. This study focuses on nitrate pollution and incorporates reaction types and sorption processes in the simulation. To model the contaminant, the first-order irreversible decay reaction and linear sorption were selected. A critical aspect of this setup was to establish the simulation's start time, which is essential for calibrating groundwater flow parameters. In this study, the initial simulation time was set to align with the first observed groundwater head on March 1, 2024.

The second step in building a conceptual model was to define what conceptual modeling entailed. In this step, the Selgi Watershed served as a boundary map for the model domain for simulating groundwater flow and contaminant transport. Establishing the conceptual structure of the model was an important part of its development. The actual geological configuration of the watershed was used to establish the number of layers in the model. This study regarded the upper portion of the aquifer up to 60 meters from the ground as a single-layer unconfined aquifer based on the well completion report shown in Figure 3. This decision was made because some wells reached a maximum depth of 60 meters below ground level. Figure 4 illustrates the 3D representation of the developed conceptual model for the study area.

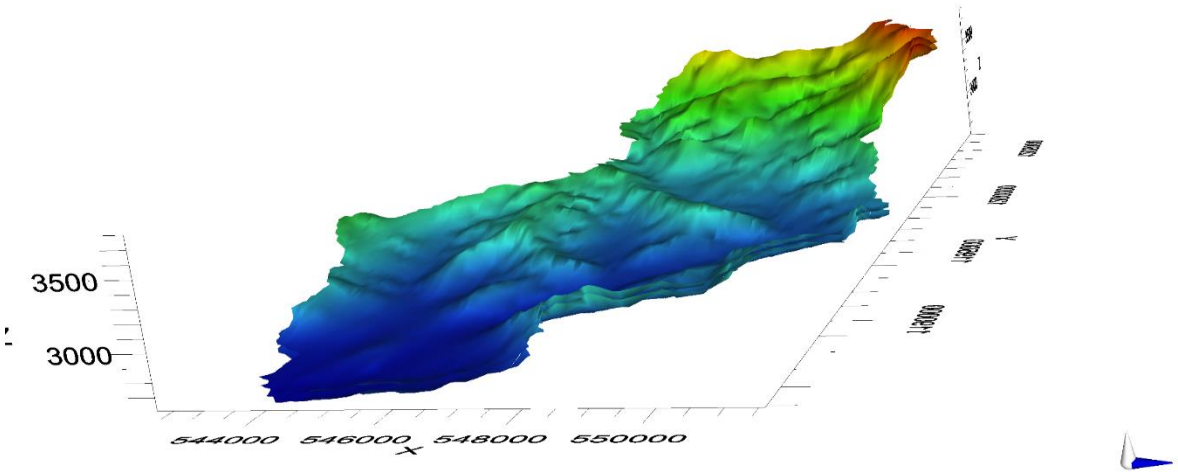

Figure 4. Conceptual model 3D view

2.3.2 Boundary Condition and Model Discretization

Before running the model, it is essential to complete critical steps such as fixing boundary conditions and model discretization. MODFLOW Flex offers various boundary condition packages, but at least one boundary condition must be defined to successfully run MODFLOW. The number of boundary conditions used is determined by modeling objectives and data availability. The number of boundary conditions applied influences the speed at which the model converges and can enhance its accuracy. In this investigation, the Recharge and River packages were selected as boundary conditions to run the model.

This study utilized monthly rainfall data from the CHIRPS (Climate Hazards Group InfraRed Precipitation with Station data) satellite, retrieved from Google Earth engine, covering the period from 2002 to 2024. The Kabe rainfall station had significant gaps in its data, so CHIRPS satellite data were chosen because of the absence of rainfall stations in the research area. Ahmed et al. (2024), Hordofa et al. (2021), and the Ethiopian Meteorological Institution recognized and validated the reliability of CHIRPS satellite data. This data served as the basis for calculating the recharge rate in the research region. An empirical estimation method was employed to determine

the recharge rate (Deribe et al., 2024). The average recharge rate derived from the four empirical formulas was used to establish the overall recharge rate as presented in Table 2.

Table 2. Recharge rate determination

Year	Annual Rianfall	Krishna R=0.25(p-400) [mm]	Groundwater Estimation Committee Norms (R=0.15*P)	Chaturvedi Formula R=1.35(p-14) ^0.5 [mm]	Bredenkamp et al R=0.32(P-360) [mm]	Average [mm]
2002	975.01	143.75	146.25	41.85	196.80	132.16
2003	1115.11	178.78	167.27	44.80	241.64	158.12
2004	993.63	148.41	149.04	42.25	202.76	135.62
2005	1081.01	170.25	162.15	44.10	230.72	151.81
2006	1266.08	216.52	189.91	47.77	289.95	186.04
2007	1156.20	189.05	173.43	45.63	254.79	165.72
2008	942.26	135.56	141.34	41.13	186.32	126.09
2009	1003.73	150.93	150.56	42.47	205.99	137.49
2010	1401.53	250.38	210.23	50.29	333.29	211.05
2011	938.27	134.57	140.74	41.04	185.05	125.35
2012	1098.60	174.65	164.79	44.46	236.35	155.06
2013	1314.43	228.61	197.17	48.68	305.42	194.97
2014	1060.51	165.13	159.08	43.67	224.16	148.01
2015	716.62	79.16	107.49	35.78	114.12	84.14
2016	1434.36	258.59	215.15	50.88	343.79	217.10
2017	1397.55	249.39	209.63	50.21	332.02	210.31
2018	1307.51	226.88	196.13	48.55	303.20	193.69
2019	1379.86	244.97	206.98	49.89	326.36	207.05
2020	1350.55	237.64	202.58	49.35	316.98	201.64
2021	1316.77	229.19	197.51	48.73	306.17	195.40
2022	1015.77	153.94	152.36	42.73	209.85	139.72
2023	1175.56	193.89	176.33	46.01	260.98	169.30
2024	1464.46	266.11	219.67	51.41	353.43	222.66
Average	1169.80	192.45	175.47	45.73	259.14	168.20
Variance		294.14	26.46	7499.37	4135.08	
Recharge Coefficient		16.44	14.99	16.50	22.13	15.76

Key, R= recharge

The study area is bounded by two rivers located in the eastern and western parts of the watershed. These rivers flow from north to south and eventually merge. The Emey River is a tributary of the

main river, Selegi. Both rivers were taken as river boundary conditions in this study, and Equation 1 was used to determine the river conductance (Deribe et al., 2024).

$$C = \frac{K^b * L * w}{M} \quad (1)$$

In this context, Kb represents the hydraulic conductivity of the riverbed, while L indicates the length of the river at the node of the cell. Additionally, W refers to the width of the river within the cell, and M signifies the thickness of the riverbed layer.

The way the model is discretized influences the convergence criteria, making it essential to determine the grid type and size before initiating any numerical modeling. In this study, a grid size of 100 meters by 100 meters was used, comprising 312 columns and 740 rows, which provides a high resolution for simulating MODFLOW Figure 5.

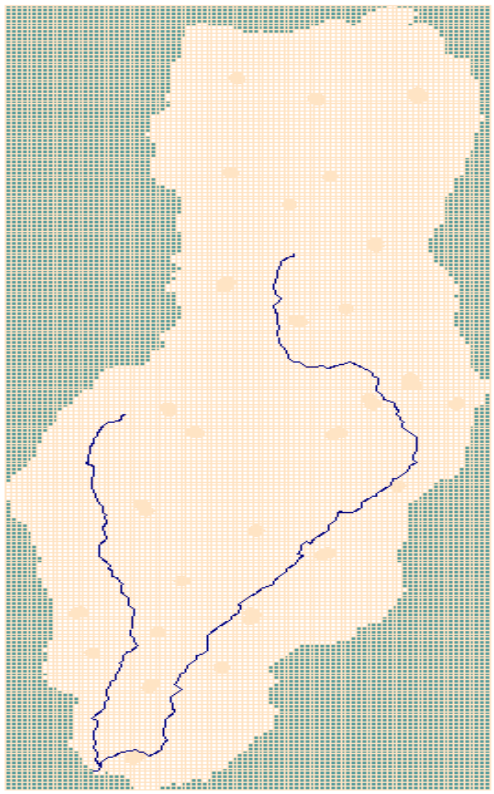

Figure 5 Model grid cell (100*100m) and selected pilot Points and Rivers

2.3.3 Numerical Model Development

After defining the boundary conditions in Visual MODFLOW, the next step is to choose the grid type and export the conceptual model to a numerical model. In this study, we utilized a finite difference grid type to simulate both hydraulic head and contamination. During this step, both flow and contaminant simulation were governed by finite difference numerical equations.

i. Groundwater flow Models

Groundwater flow simulation was a primary process before simulating mass transport. Partial differential equations govern groundwater flow in fully saturated soil (Equation 2) (Karatzas, 2017).

$$\frac{\partial}{\partial_x}\left(K_X\frac{\partial h}{\partial_X}\right)+\frac{\partial}{\partial_y}\left(K_y\frac{\partial h}{\partial_y}\right)+\frac{\partial}{\partial_z}\left(K_z\frac{\partial h}{\partial_z}\right)-s\frac{\partial h}{\partial t}+\sum_{i=1}^{r}Q_i\delta(x-x_i)\delta(y-y_i)\delta(z-z_i)=0 \qquad (2)$$

where K_y= stands for hydraulic conductivity in the y direction (LT^{-1}), K_x= for hydraulic conductivity in the x direction (LT^{-1}), K_z= for hydraulic conductivity in the z-direction (LT^{-1}), S= for the specific storage coefficient (L^{-1}), Qi= for the source/sink term at point i (L^3 3 T^{-1}), and δ= for the delta function r for the number of sources/sinks.

$$V_x=\left(K_X\frac{\partial h}{\partial_X}\right),V_y=\left(K_y\frac{\partial h}{\partial_X}\right),V_Z=\left(K_z\frac{\partial h}{\partial_X}\right) \qquad (3)$$

Where, V_x, V_y, V_z denotes the x, y and z components of Darcy velocity, respectively [LT^{-1}]

Setting up groundwater parameters is a vital step in groundwater flow simulation. In this study, we determined the initial parameters through a trial-and-error method during the calibration process. For the initial head, we used the model top or the grid top. For initial hydraulic conductivity, we referenced a value of 0.03 m/d obtained from the well completion report. This study applied the default value of the model V_x=V_y, but V_z=0.1V_x

ii. MT3DMS Models

After successfully simulating groundwater flow modeling, the next step in Visual MODFLOW Flex involves a mass transport process. To model three-dimensional mass transfer in the study area, we selected the modular three-dimensional multi-species transport model, known as MT3DMS. The behavior and movement of pollutants for species k in three-dimensional, transient

groundwater flow systems can be described using the following partial differential equation (equation 4). (Chunmiao Zheng, 1999).

$$\frac{\partial(\theta C^k)}{\partial t} = \frac{\partial}{\partial x_i}\left(\theta D_{ij}\frac{\partial C^k}{\partial x_j}\right) - \frac{\partial}{\partial x_i}\left(\theta v_i C^k\right) + q_s C_s^k + \sum R \quad (4)$$

Where θ denotes porosity of the subsurface medium, C^k is the dissolved concentration of species k, t is time, $x_{i,j}$ represents distance along the coordinates $D_{i,j}$ denotes the hydrodynamic dispersion coefficient tensor, v_i is the velocity related to Darcy flux q_s is volumetric flow rate, C_s^k is the concentration of source sink flus for species k, and ∑R chemical reaction

The mass balance statement to consider both dissolved and sorbed phases, equation 4 was converted into (5)

$$\partial\frac{\partial C}{\partial t} + \rho_b\frac{\partial \bar{C}}{\partial t} = \frac{\partial}{\partial x_i}\left(\theta D_{ij}\frac{\partial C^k}{\partial x_j}\right) - \frac{\partial}{\partial x_i}\left(\theta v_i C^k\right) + q_s C_S + \acute{p}_s C - \lambda_1\theta C - \lambda_2\rho_b\bar{C} \quad (5)$$

Where ρ_b bulk density of the surface medium, $\bar{C}$ concretion of species on the subsurface solids, λ_1 first order reaction rate for the dissolved phase, λ_2 first order reaction rate for the orbed (solid) phase and $\acute{p}_s$ $=\partial\theta/\partial t$ is the rate of change in transient groundwater storage.

The dispersion D_{ij} terms are defined as:

$$D_{xx} = \left(a_L {V_x}^2 + a_T {V_y}^2 + a_V {V_z}^2\right)/V + D_M \quad (6)$$

$$D_{yy} = \left(a_T {V_x}^2 + a_L {V_y}^2 + a_V {V_z}^2\right)/V + D_M \quad (7)$$

$$D_{zz} = \left(a_V {V_x}^2 + a_V {V_y}^2 + a_L {V_z}^2\right)/V + D_M \quad (8)$$

$$D_{yx} = D_{xy} = (a_L + a_T)V_x V_y/V \quad (9)$$

$$D_{yz} = D_{zy} = (a_L - a_v)V_y V_z/V \quad (10)$$

$$D_{xz} = D_{zx} = (a_L - +a_v)V_x V_z/V \quad (11)$$

Where D_M is the molecular diffusion coefficient (L^2 T^{-1}), a_L is longitudinal dispersity (L), a_T is transverse dispersity (L), a_V is vertical dispersity (L), and V is the velocity of groundwater flow. Linear isotherm or equilibrium-controlled sorption assumes the sorbed $(\overline{C})$ is directly proportional to the dissolved concentration.

$$\bar{C} = K_d C \quad (6)$$

Where K_d is the distribution coefficient

The first-order irreversible rate reaction term included in the governing equation, - $(\lambda_1 \theta C - \lambda_2 \rho_b \bar{C})$, represents the mass loss of both the dissolved phase *(C)* and the sorbed phase **($\bar{C}$).** The rate constant is usually given in terms of the half-life,

$$\lambda = ln2/t_{1/2} \quad (7)$$

where $t_{1/2}$ is the half-life of radioactive or biodegradable materials (i.e., the time required for the concentration to decrease to one-half of the original value).

Owing to the properties of nitrate contaminant species, this study considered the processes of advection, dispersion, sorption, and reaction. The molecular dispersity of nitrogen in free water, measured at 0.000432 m²/d, was utilized in this study (Huan et al., 2020). The other parameters, such as porosity, bulk density, sorption (using a linear isotherm sorption model), reaction (first-order irreversible decay), and longitudinal dispersion, were determined through a trial-and-error method during the calibration process of the model. The distribution coefficient values (K_d) for sorption ranging from 0 to 3.3×10^{-6} l/mg/l were observed. Denitrification within the aquifer was considered a chemical decay process in mass transport modeling and was modeled using a first-order rate. The nitrate half-life ranged from 1.1 to 3.0×10^{-4} d^{-1} (Zhang et al., 2020). The ratios of horizontal (transversal) and vertical dispersion to longitudinal dispersion were set to model default values of 0.1 and 0.01, respectively.

2.3.3 Model Translation

After converting the conceptual model into a numerical model, the next step is to perform model translation before running Visual MODFLOW Flex. This step is crucial for both flow and transport modeling. During this procedure, you need to select the model engine, solver, time steps, and output controls. It is often performed after modifying parameter values and is particularly important for manual calibration. The PEST model utilized the MODFLOW 2005 flow model for automatic calibration in the Visual MODFLOW Flex 2015 software to simulate hydraulic head. The Time Steps option is only available when operating in PEST mode, so we utilized transient flow conditions. This research modeled groundwater flow over a single stress period divided into 12-time steps based on the observed data collected. We employed the default configurations of the MODFLOW 2005 solver, specifically using the Conjugate-Gradient Package (CGP).

Effective porosity was chosen while translating the transport model because this study employed an advection-dominated simulation. The Total Variation Diminishing (TVD) method, an advection-based technique, was used in this work to model transport. The very conservative TVD method regulated the advection term using the Universal Limiter for Transient Interpolation Modeling of the Advective Transport Equations (ULTIMATE) technology, first introduced by Leonard (1988). The TVD methodology computed the advection component independently of the other components in the transport equation, just like particle-based systems did. It is essential to note that the TVD method is explicit, which places a stability constraint on the time step size. Although the results may show slight oscillations and numerical dispersion in situations with abrupt concentration fronts.

2.3.5 Model Calibration, Sensitivity Analysis, and Validation

In numerical groundwater modeling, calibration is a challenging stage (Valivand & Katibeh, 2020). The Visual MODFLOW Flex model offers both manual and automatic calibration techniques. PEST, an automated technique, was developed by Doherty, in 1994. PEST is a reliable method for conducting sensitivity assessments of groundwater parameters and calibrating MODFLOW. Calibration involves adjusting the parameters of the model with observed data to ensure they closely align. Validation, on the other hand, confirms the accuracy of these calibrated parameters and evaluates their performance against a new dataset. Additionally, a sensitivity analysis is performed to identify which parameters significantly influence the accuracy of the model, allowing for more effective calibration.

This study used one year of monthly observations of groundwater levels from eighteen hand-dug wells, ranging from March 2024 to February 2025, to evaluate model performance. The data from twelve of these wells were used for calibration, while the remaining six wells were reserved for validation. One-third of the validation data was allocated for validation, while the other two-thirds were employed for calibration. Following the successful calibration and validation of the groundwater flow model, the next phase in the groundwater modeling process involved calibrating the transport model. For this calibration, a manual method was used, employing observed nitrate concentration data collected from twelve hand-dug wells over three months.

The well-known parameter estimation and predictive analysis program PEST, created by Dr. John Doherty at Watermark Computing, was integrated with Visual MODFLOW Flex (Christensen &

Doherty, 2008). The PEST model conducts sensitivity analysis and parameter calibration through the following procedures.

1. Define observations and assign weights. In these steps, the system provides options to choose the observation type. This study selects observed head values for calibration and assigns the same weight to each well. contaminant
2. Establish Parameters (Property Zones, Boundary Conditions): During the "Define PEST Parameters" phase, choose the types of model inputs to be incorporated into this analysis. In this stage, the analysis focuses on hydraulic conductivity in both horizontal and vertical orientations, along with specific storage and specific yield parameters designated as the MODFLOW parameters. Furthermore, the range is established according to the initial values of the parameters.
3. Define Pilot Points: To overcome the drawbacks of traditional model calibration techniques, which tend to be labor-intensive, this study utilizes a set of pilot points to describe the distribution of transmissivity within the model domain. For this purpose, 63 pilot points were selected uniformly across the watershed, from upstream to downstream (Fig. 2).
4. Define Kriging Variograms: The default settings were accepted to run the PEST model.
5. Define PEST Run Settings: At this stage, the modeler selects either parameter estimation or sensitivity analysis. In this study, both sensitivity analysis and parameter estimation were conducted. To run PEST, this study used Tikhonov Regularization because this method achieves numerical stability by adding extra information or constraints to the model.
6. Analyze Results: This step presents the results of the PEST Model, and it is possible to export the results.
7. After running the model, the calibrated parameters can be used in the newly established post-run numerical model.

The PEST model was calibrated and its performance validated using performance metrics like Standard Error of the Estimate (SEE), Root Mean Squared error (RMS), Normalized Root Mean Square (NRMS), and correlation Coefficient (R^2).

The variability of the residuals around the expected residual value was measured by the Standard Error of the Estimate (SEE), as indicated in Equation (12).

$$SEE = \sqrt{\frac{\frac{1}{n-1}\sum_{i=1}^{n}(R_i-\bar{R})^2}{n}} \quad (12)$$

Where R_i is the calibration residual calculated as (equation 13),

$$R_i = h_c - h_o \quad (13)$$

n denotes the total amount of observed data, h_c is the estimated head value, and h_o is the observed head value of transport modelling, instead of h_o and h_c to calibrate concentration Co and C_c were used to express the observed and estimated concentration, respectively. $\bar{R}$ was the residual mean calculated as (eq.14)

$$\bar{R} = \frac{1}{n}\sum_{i=1}^{n} R_i \quad (14)$$

Then the Root Mean Square error (RMSE) is calculated as

$$\bar{R} = \sqrt{\frac{1}{n}\sum_{i=1}^{n} {R_i}^2} \quad (15)$$

The Normalized Root Mean Squared is the RMS divided by the maximum difference in the observed head values, equation 17.

$$Normilized\ RMS = \frac{RMS}{(h_o)_{max} - (h_o)_{min}} \quad (16)$$

The Normalized RMS is represented as a percentage and offers a more precise assessment of fit compared to the standard RMS, since it considers the scale of the possible data range.

The Correlation Coefficient (R) is determined by dividing the covariance (Cov) between the computed results and the actual results at chosen data points by the product of their standard deviations.

$$Cor\ (R^2) = \frac{\frac{1}{n}\sum_{i=1}^{n}(h_c - \bar{h}_c)(h_o - \bar{h}_o)}{\sqrt{\frac{1}{n}\sum_{i=1}^{n}(h_c - \bar{h}_c)} * \sqrt{\frac{1}{n}\sum_{i=1}^{n}(h_o - \bar{h}_o)}} \quad (17)$$

Where $\bar{h}_c$ and $\bar{h}_o$ are the averages of calibrated and observed heads, respectively

The lower SEE, RMS, and Normalized RMS error values indicated a more accurate model performance. The correlation coefficient ranges from 0 to 1, with a value closer to 1 indicating better model performance. The workflow of this study is illustrated in Figure 6.

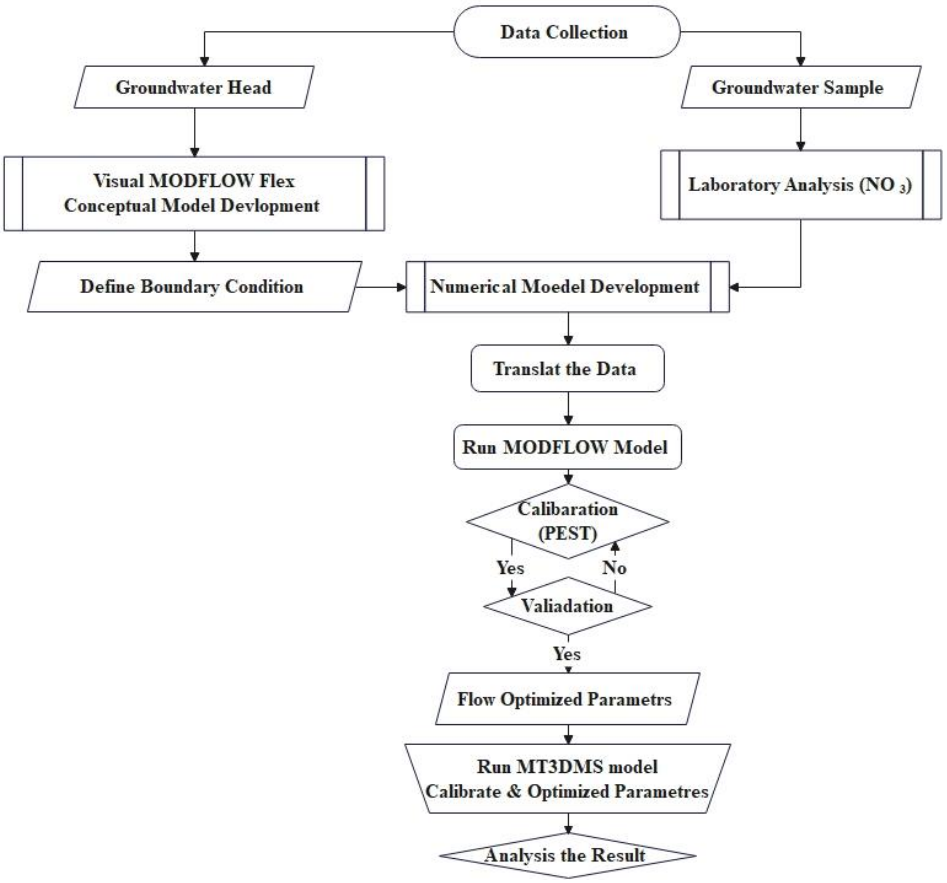

Figure 6. MODFLOW and Transport Modeling Flow Chart

3. RESULT AND DISCUSSION

3.1 Observed Time Series Data Interpretation

As shown in Figure 7, the fluctuations in the average groundwater table depth corresponded to the monthly precipitation variations obtained from the CHIRPS satellite data. A deep-water table was recorded in April 2024 while a very shallow water table was observed in August 2024. This was attributed to increased precipitation during that month. This study confirmed that groundwater fluctuations in the area were driven by recharge, indicating the shallow groundwater being part of an unconfined aquifer. On the other hand, while working with a confined aquifer, the recharge source was usually located a distance from the well. This caused a delay in the response to precipitation.

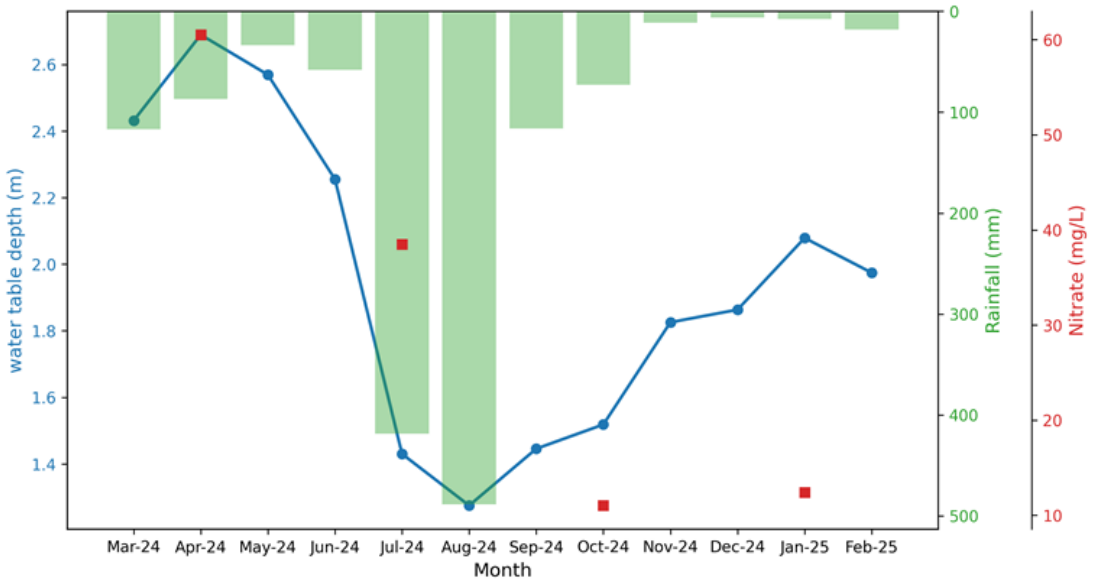

Figure 7. Average groundwater table fluctuation, Rainfall depth, Nitrate concentration

In contrast to the dry season, the average nitrate concentration was lower during the summer. This reduction occurred because groundwater recharge diluted the nitrate content. As a result, nitrate concentration tended to rise as the next dry season approached, as illustrated in Figure 7. This finding aligned with previous studies which suggested that nitrate concentrations decreased during the wet season (Wang et al., 2024; Mussa, 2025).

3.2 Groundwater Flow Model Sensitivity Analysis, Calibration, And Validation

Before calibrating the groundwater flow parameters, the PEST Model automatically identifies the sensitive parameters. In the PEST Model, the parameters listed for calibrated defaults include horizontal hydraulic conductivity (Pg1), vertical hydraulic conductivity (Pg2), specific storage (Pg3), and specific yield (Pg4). The results shown in Figure 8 indicate that horizontal hydraulic conductivity is the most sensitive parameter, corresponding to the label Pg1. The other parameters, Pg2 (vertical hydraulic conductivity), Pg3 (specific storage), and Pg4 (specific yield), were kept constant. Honnannanavar et al. (2023) stated that hydraulic conductivity is a sensitive parameter.

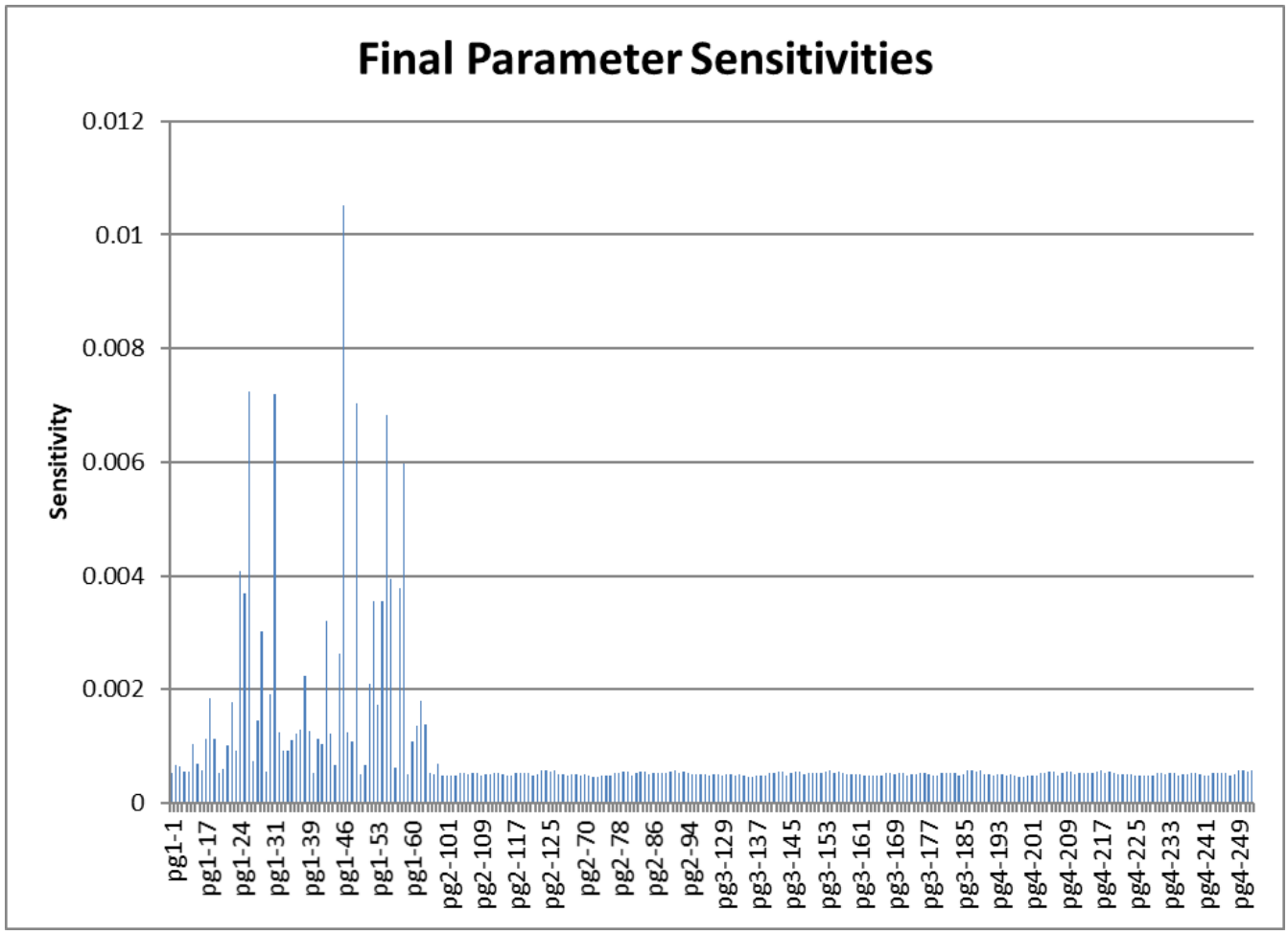

Figure 8. Sensitivity analysis

Groundwater flow characteristics were calibrated in this study using both manual and advanced methods, including the PEST Model. The results showed a standard error estimate (SEE) of 5.49, a root mean square error (RMSE) of 34.0, a normalized RMSE of 20.23%, and a correlation coefficient (R^2) of 0.98, indicating the model's effectiveness (see Figure 9). Nagaraj and Shankar's (2025) study confirmed that the R^2 value was 0.98 after calibrating the groundwater flow simulation over 365 days. The corresponding measurements included a standard error of estimate (SEE) of 3.72 meters, a root mean square error (RMSE) of 27.87 meters, and a normalized RMSE of 6.33%. Thus, this study supported the conclusion that the model operates satisfactorily.

After lengthy iterations, the output of the PEST Model showed that the optimal horizontal hydraulic conductivity ranged between 0.01 and 0.15 m/d. Other parameters remained constant

throughout the model iterations: vertical conductivity at 0.003 m/d, specific storage at 0.00001/m, and specific yield at 0.19.

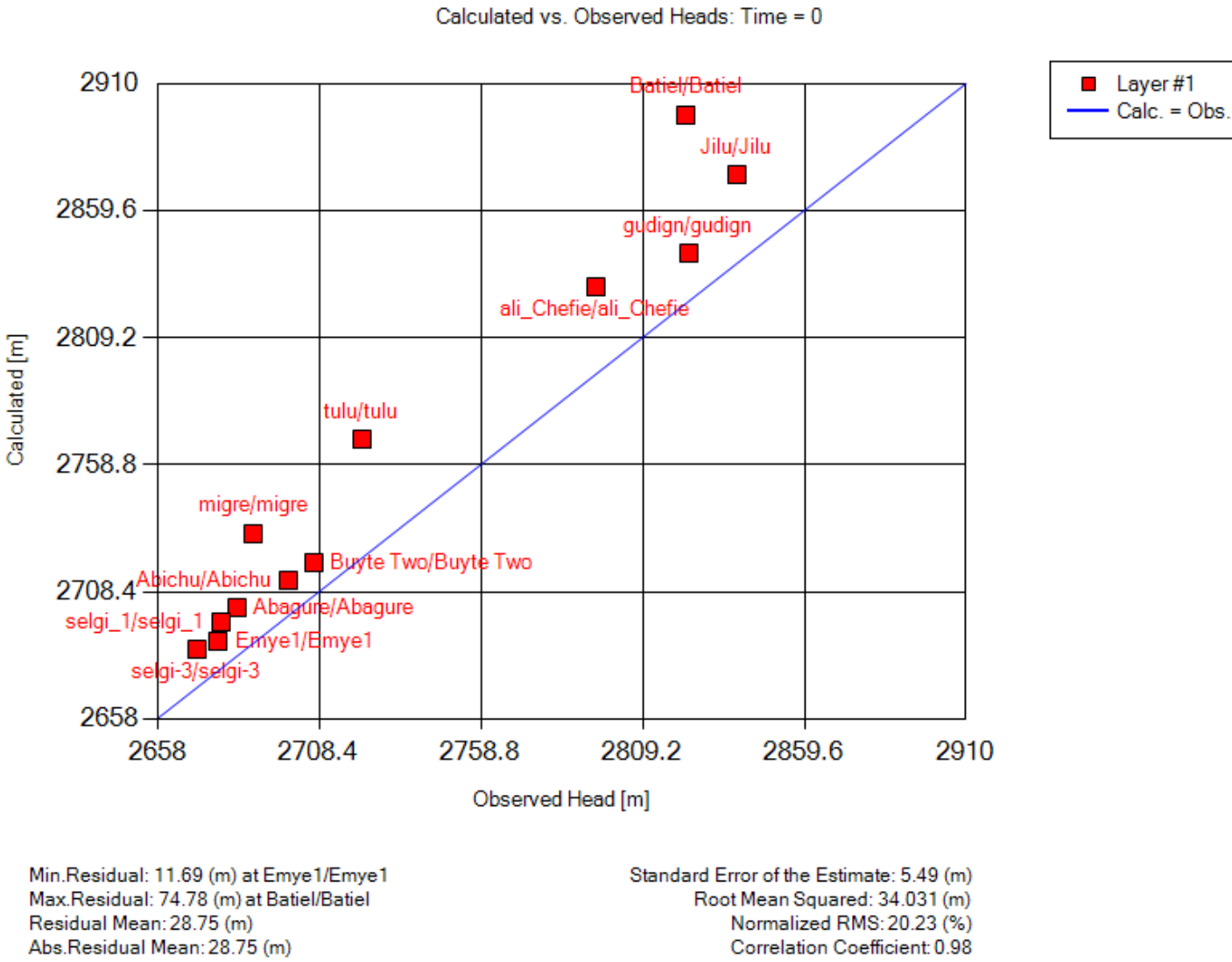

Figure 9. MODFLOW calibration scatter plot

Model verification was performed to determine whether the calibrated model parameters accurately predicted the fresh well head data set. Figure 10 shows that the model performed well, with performance measures including SEE of 11.8, RMSE of 22.29, adjusted RMSE of 20.33%, and R^2 of 0.87.

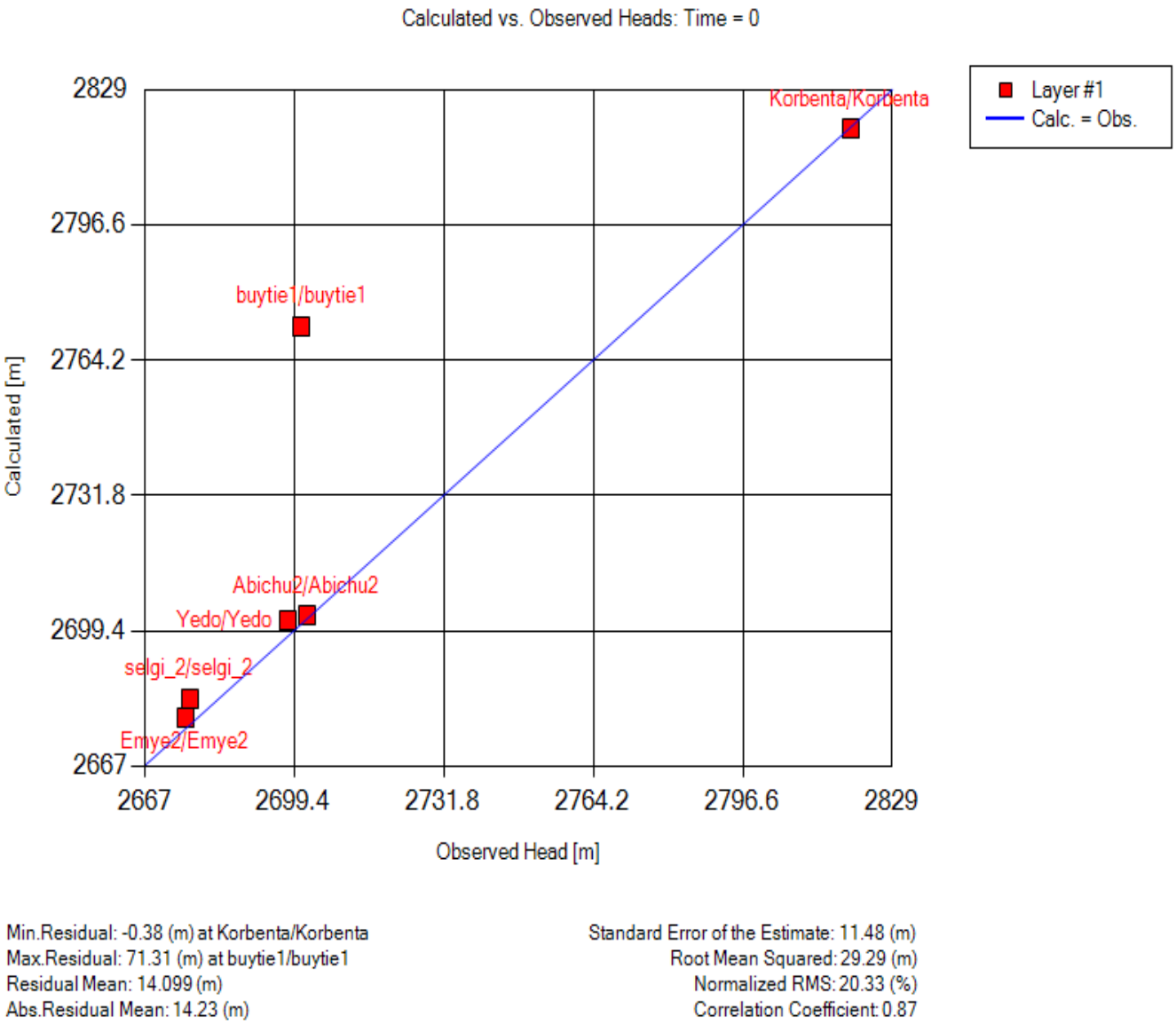

Figure 10. MODFLOW validation scatter plot.

3.3 Transport Model (MT3DMS) Calibration

After calibrating and validating the flow model, the transport model was calibrated using the optimized groundwater flow model parameters as a step. The transport model calibration was conducted using a manual calibration (Trial and Error) method. The calibration results of the MTD3MS Model were successful, with SEE = 2.97, RMSE = 26.27, Normalized RMSE = 29.93, and $R^2 = 0.78$, as illustrated in Figure 11. This indicates that the model performs moderately well.

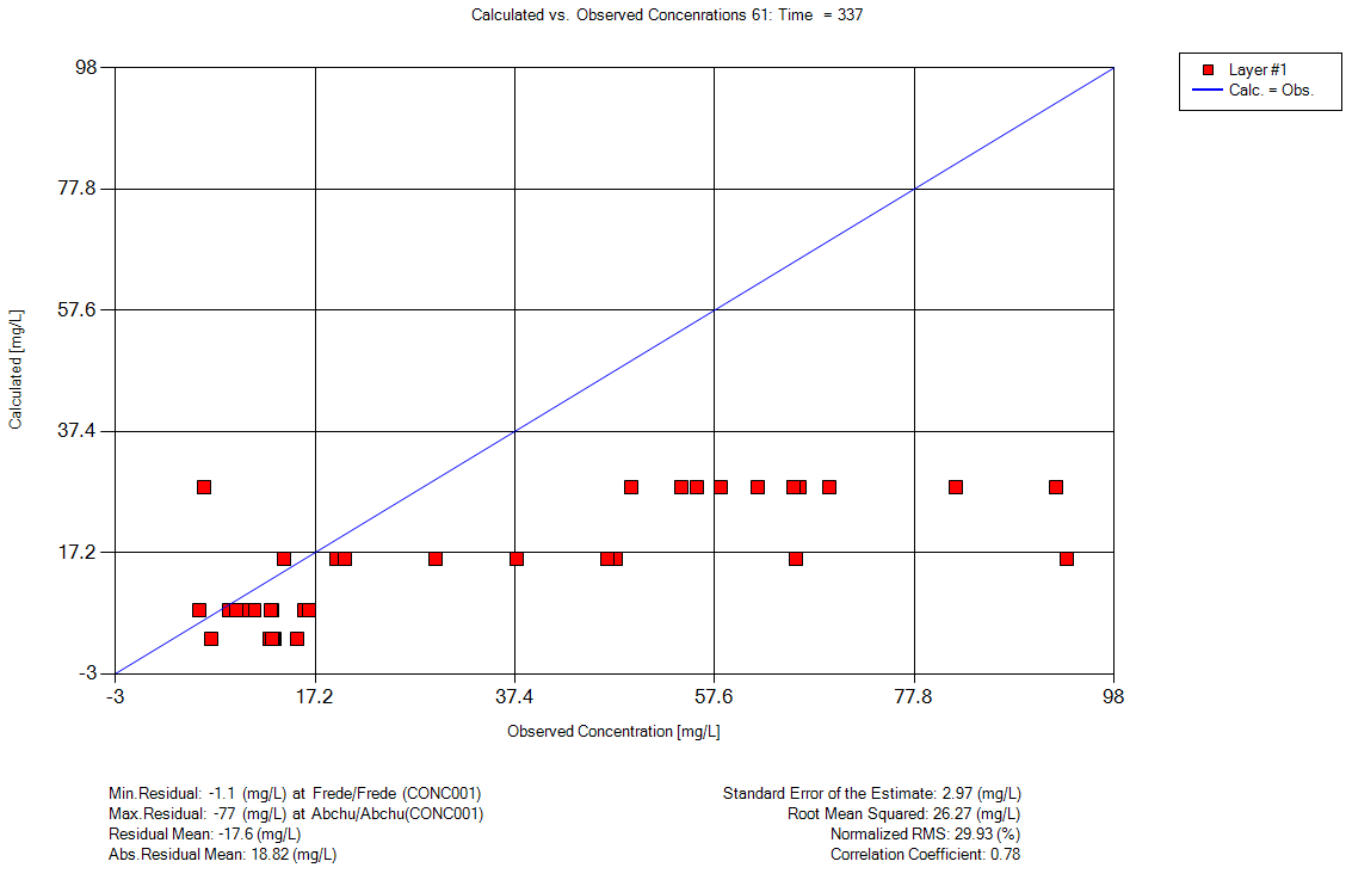

Figure 11. Transport model calibration scatter plot

Based on the model results, the estimated longitudinal parameter for the nitrate plume was found to be 100 meters. This finding was consistent with a prior research by Huan et al. (2020), which indicated that groundwater systems could exhibit nitrate concentrations with longitudinal depressions extending up to 100 meters. To gain a clearer understanding of nitrate behavior in this environment, the distribution coefficient for nitrate, referred to as Kd, was calibrated to a value of 0.00001. Additionally, the reaction rate was determined to be 0.001. This indicates that the average denitrification rate was observed. That is to say, nitrate had low adsorption to soil or rock particles, and microbes may convert nitrate into nitrogen gas at a moderate rate.

3.4 Groundwater Head and Contaminated Concentration Level

Figure 12 presents the results of groundwater head simulations carried out over 12-time steps within a single stress period of 365 days. The data indicated a notable variation in groundwater

levels throughout the watershed, with the upper areas consistently showing higher groundwater heads than the lower regions. However, when these levels were analyzed in relation to ground elevation, the lower regions had, on average, shallower groundwater depths than the upper areas.

Additionally, a hydrological dynamic was observed at the riverbanks, where the groundwater table rose above the riverbed level. This situation showed that groundwater was flowing into the river, which helped to maintain its base flow. Consequently, this interaction between groundwater and surface water supported the consistent flow of the river, which was crucial for preserving biological balance and supporting regional aquatic ecosystems. Understanding these connections was crucial for effective watershed management and for predicting the impacts of various stresses on both groundwater and surface water resources.

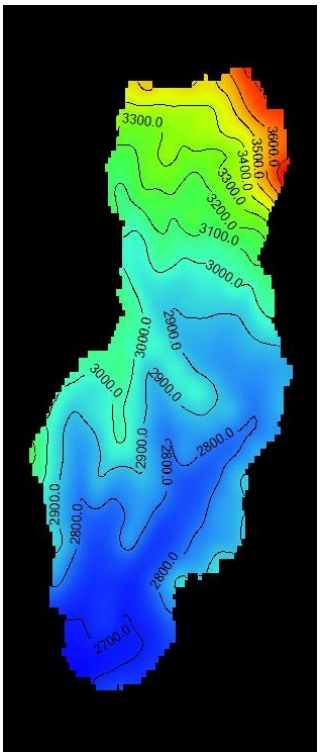

Figure 12. Map of simulated groundwater head (m) above sea level

The analysis of nitrate concentration across the watershed indicated that there was only a minor change observed throughout the entire area after 365 days. This lack of variance might be attributed to the dominance of an advective transport model, where the flow rate is closely aligned with

horizontal hydraulic conductivity. Notably, the hydraulic conductivity within the watershed varied slightly, ranging from 0.01 to 0.15 m/day. Hydraulic conductivity affected the travel time of contaminants (Comolli & Dentz, 2017). In an advective-dominated transport model, there is relatively low transverse horizontal and vertical dispersity (Bergvall et al., 2011).

As illustrated in Figure 13, the simulated nitrate concentrations were relatively higher in the northeastern and certain southwestern parts of the research area. This increase could be linked to the geological characteristics of these regions, which were primarily composed of weathered rock and loam soil. These materials contributed to a low potential for attenuation. In contrast, the lower portion of the research area exhibited comparatively lower nitrate concentrations, predominantly owing to the presence of heavy clay soils which provided better filtration and retention of nitrates.

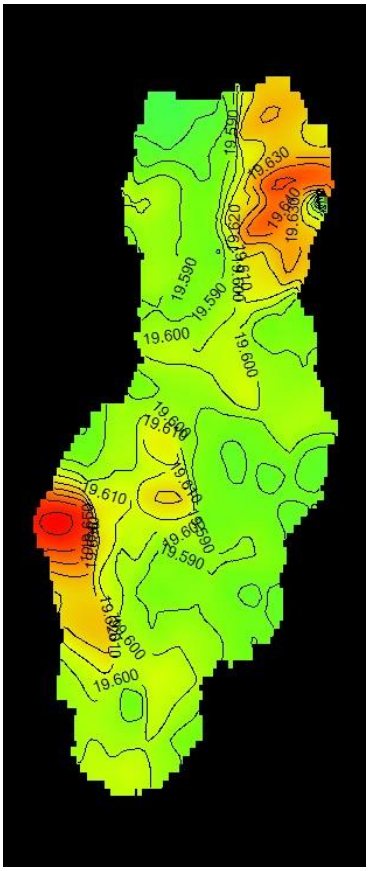

Figure13. Simulated nitrate concentration (mg/l)

Despite some observed changes throughout the entire watershed, the vulnerability of the aquifer to nitrate contamination remained a significant concern. The concentration of nitrate exceeded 19

mg/l, which indicated contamination, while the natural concentration level was typically below 3 mg/l (Kirlas et al., 2023).

The researchers collected nitrate concentration data at four distinct time intervals, spaced three months apart. Simultaneously, groundwater head measurements were taken for over 12 months. However, the dataset was not sufficient to effectively replicate nitrate concentrations. An extended time series of data was needed to create a more realistic and accurate simulation of nitrate dynamics within the groundwater system. This longer timeframe allowed for a more detailed investigation into the factors driving fluctuations in nitrate levels and enhanced understanding of the hydrogeological processes involved.

4. CONCLUSION

Groundwater and contamination transport modeling were utilized in this study to assess groundwater levels and determine the optimal parameters for evaluating pollutant concentrations. The results indicated that hydraulic conductivity significantly affected groundwater dynamics. Higher hydraulic heads were observed in the upper part of the watershed, and in specific areas of the survey, particularly along riverbanks, the hydraulic head exceeded the actual ground elevation. This phenomenon demonstrated that the river functioned as a gaining feature, transferring groundwater into its base flow. Furthermore, because of the uniform hydraulic conductivity of the aquifer and the slow movement of groundwater, changes in nitrate concentrations were minimal. The performance of the model was assessed using various metrics in the Visual MODFLOW Flex Model, incorporating both automated calibration (PEST) and manual calibration. The results showed strong performance during the calibration and validation phases of the flow model, with a correlation coefficient of 0.98 during calibration and 0.89 during validation. However, owing to data limitations, only the calibration of nitrate concentration was conducted, resulting in a correlation coefficient of 0.78. This study emphasized the importance of collecting longer time series data, including groundwater levels and contaminant concentrations, to improve model accuracy and understand how aquifers respond to contaminants. This study might assist decision-makers and researchers in establishing mitigation measures to reduce pollution caused by fertilizer application, thereby mitigating groundwater pollution in the study area and other regions of the country.

REFERENCES

Ahmed, J. S., Buizza, R., Dell, M., Teferi, A., & Pè, M. E. (2024). Evaluation of ERA5 and CHIRPS rainfall estimates against observations across Ethiopia. *Meteorology and Atmospheric Physics*, *136*(3), 1–15. https://doi.org/10.1007/s00703-024-01008-0

Ayenew, T., Demlie, M., & Wohnlich, S. (2008). Application of numerical modeling for groundwater flow system analysis in the Akaki catchment, central Ethiopia. Mathematical geosciences, 40(8), 887-906.

Bergvall, M., Grip, H., Sjöström, J., & Laudon, H. (2011). Modeling subsurface transport in extensive glaciofluvial and littoral sediments to remediate a municipal drinking water aquifer. Hydrology and Earth System Sciences, 15(7), 2229-2244.

Christensen, S., & Doherty, J. (2008). Predictive error dependencies when using pilot points and singular value decomposition in groundwater model calibration. *Advances in Water Resources*, *31*(4), 674–700. https://doi.org/10.1016/j.advwatres.2008.01.003

Chunmiao Zheng, P. P. W. (1999). 20000214 046. In *MT3DMS: A Modular Three-Dimensional Multispecies Transport Model for Simulation of Advection, Dispersion, and Chemical Reactions of Contaminants in Groundwater Systems; Documentation and User's Guide* (20000214 046; Issue December).

Comolli, A., & Dentz, M. (2017). Anomalous dispersion in correlated porous media: a coupled continuous time random walk approach. The European Physical Journal B, 90(9), 166.

Deribe, W., Deressa, G., Abebe, S., & Solomon, G. (2024). *Groundwater modeling and estimation of the safe pumping rate for the sustainable use of groundwater resources in Kombolcha town , upper Borkena watershed , Ethiopia*. *24*(8), 2704–2719. https://doi.org/10.2166/ws.2024.159

Filippis, G., Ercoli, L., & Rossetto, R. (2021). A spatially distributed, physically-based modeling approach for estimating agricultural nitrate leaching to groundwater. Hydrology, 8(1), 1–25. https://doi.org/10.3390/hydrology8010008

Hariharan, V., & Uma Shankar, M. (2017). A review of visual modflow applications in groundwater modelling. *IOP Conference Series: Materials Science and Engineering*, *263*(3). https://doi.org/10.1088/1757-899X/263/3/03202.

Honnannanavar, A., Patil, N. S., & Patil, V. (2023). Groundwater Flow Modeling of A Microwatershed using Visual Modflow Flex. *Current World Environment*, *18*.

Hordofa, A. T., Leta, O. T., Alamirew, T., Kawo, N. S., & Chukalla, A. D. (2021). *Performance Evaluation and Comparison of Satellite-Derived Rainfall Datasets over the Ziway Lake Basin , Ethiopia*.

Huan, H., Hu, L., Yang, Y., Jia, Y., Lian, X., & Ma, X. (2020). Groundwater nitrate pollution risk assessment of the groundwater source fi eld based on the integrated numerical simulations

in the unsaturated zone and saturated aquifer. *Environment International*, *137*(July 2019), 105532. https://doi.org/10.1016/j.envint.2020.105532

Karatzas, G. P. (2017). Developments on Modeling of Groundwater Flow and Contaminant Transport. *Water Resources Management*, *31*(10), 3235–3244. https://doi.org/10.1007/s11269-017-1729-z

Kirlas, M. C., Karpouzos, D. K., Georgiou, P. E., & Theodossiou, N. (2023). A GIS-Based Comparative Groundwater Vulnerability Assessment Using Modified-DRASTIC, Modified-SINTACS and NV Index in a Porous Aquifer, Greece. *Environments - MDPI*, *10*(6). https://doi.org/10.3390/environments10060095

Kumar, M., Singh, S. K., Kundu, A., Tyagi, K., Menon, J., Frederick, A., Raj, A., & Lal, D. (2022). GIS-based multi-criteria approach to delineate groundwater prospect zone and its sensitivity analysis. *Applied Water Science*, *12*(4), 1–14. https://doi.org/10.1007/s13201-022-01585-8

Leonard, B. P. (1988). *Universal Limiter for Transient Interpolation Modeling of the Advective Transport Equations : The ULTIMATE Conservative Difference Scheme*.

Mrinal Kumar Singh, & Susmita, G. (2022). Groundwater flow modeling for cachar, India using MODFLOW: a case study. *ISH Journal of Hydraulic Engineering*, *28*(2), 232–242. https://doi.org/10.1080/09715010.2020.1868357

Mussa, M. M., Lohani, T. K., & Eshete, A. A. (2025). Evaluation of groundwater quality for drinking and irrigation purposes in the Gidabo watershed, Ethiopia. Heliyon, 11(15).

Nagaraj, S., & Shankar, U. (2025). Simulation of fluoride transport in groundwater using visual MODFLOW flex and Human Health Risk Assessment. *Applied Water Science*, *15*(5), 1–21. https://doi.org/10.1007/s13201-025-02454-w

National Research Council. (1993). Ground Water Vulnerability Assessment. In *Ground Water Vulnerability Assessment*. The National Academies Press. https://doi.org/10.17226/2050

Ochwach Jimrise, Okongo Mark, Ombaka Ochieng. Mathematical Modelling and Simulation of Nitrate Leaching into Groundwater. International Journal of Systems Science and Applied Mathematics. Vol. 7, No. 4, 2022, pp. 74-84.doi: 10.11648/j.ijssam.20220704.12

Sundararajan, N., & Sankaran, S. (2020). Groundwater modeling of Musi basin Hyderabad, India: a case study. *Applied Water Science*, *10*(1), 1–22. https://doi.org/10.1007/s13201-019-1048-z

Sundararaj, S., Muthukaruppan, K., Mariappan, D., & Veluswamy, K. (2022). Groundwater contaminant transport modeling using Visual MODFLOW: a case study of corporation sewage farm in South Madurai, Tamil Nadu, India. *Arabian Journal of Geosciences*, 15(18), 1538.

Tesfamichael, G. (2009). Regional groundwater flow modeling of the Geba Basin, northern

Ethiopia (Doctoral dissertation, PhD Thesis, Vrije Universiteit, Brussel (unpubl)).

Tigel Belay, Ilfios Tesfay, Abiy Ayalew, Genet Yohannes, Teferi Zewdie, Henok Bekele, Melese Tadesse, T. D. and T. A. (2010). *Basic Geoscience Mapping Core Process Geology of Woreilu Area* (Issue February).

Tsegaw, W. D., Hatiye, S. D., & Eshete, A. A. (2025). Comparative groundwater potential mapping using AHP and FR methods in the Woleka River sub-basin, Ethiopia. Water Practice & Technology, 20(7), 1661-1680.

Tsegaw, W. D., Hatiye, S. D., & Eshete, A. A. (2026). Comparative evaluation of groundwater vulnerability to pollution using DRASTIC and modified DRASTIC models: case study in Woleka sub-basin, upper Blue Nile, Ethiopia. Discover Applied Sciences.

Valivand, F., & Katibeh, H. (2020). Prediction of Nitrate Distribution Process in the Groundwater via 3D Modeling. *Environmental Modeling & Assessment*, 187–201.

Wang, D., Wu, J., Li, P., Li, L., Yang, J., Zhang, P., ... & Wang, Y. (2024). Seasonal nitrate variations, risks, and sources in groundwater under different land use types in a thousand-year-cultivated region, northwestern China. Environmental Research, 251, 118699.

Waterloo Hydrogeologic. (2009). *Visual MODFLOW Premium - Demo Tutorial*. http://trials.swstechnology.com/software/Visual_MODFLOW/2010.1/tutorials/VMOD_Airport_Tutorial.pdf

Zhang, H., Yang, R., Guo, S., & Li, Q. (2020). Modeling fertilization impacts on nitrate leaching and groundwater contamination with HYDRUS - 1D and MT3DMS. *Paddy and Water Environment*, *18*(3), 481–498. https://doi.org/10.1007/s10333-020-00796-6